International Journal of Solids and Structures 49 (2012) 445–456

Contents lists available at SciVerse ScienceDirect

International Journal of Solids and Structures

journal homepage: www.elsevier.com/locate/ijsolstr

Identification of material parameters for Drucker–Prager plasticity model for FRP confined circular concrete columns

Jia-Fei Jiang, Yu-Fei Wu *

Dept. of Civil and Architectural Engineering, City University of Hong Kong, Hong Kong

ARTICLE INFO

Article history:
Received 7 April 2011
Received in revised form 20 September 2011
Available online 12 October 2011

Keywords:
Drucker–Prager plasticity model
FRP confined concrete
Friction angle
Cohesion
Plastic dilation

ABSTRACT

Existing research works have established that Drucker–Prager (DP) plasticity model is capable of modeling stress–strain behavior of confined concrete. However, accuracy of the model largely depends on adequate evaluation of its parameters that determine the yield criterion, hardening/softening rule and flow rule. Through careful analytical studies of test results of FRP confined concrete columns under theoretical framework of the DP model, it is found that: (1) the hardening/softening rule is governed by plastic strains and the FRP stiffness ratio; (2) the friction angle decreases slightly with an increase in plastic deformation; and (3) the plastic dilation angle is a function of both axial plastic strain and the FRP stiffness ratio. Explicit models for these properties are developed from analytical studies. By implementing the proposed models in ABAQUS, finite element analyses can well predict stress–strain responses of FRP confined concrete columns.

1. Introduction

Due to complexity of concrete, a general and mature constitutive model for the material has not been developed till date. This often becomes the bottleneck in the study of concrete structures. Since empirical/semi-empirical models are limited by availability of experimental data, computational constitutive models have been attempted more extensively in recent years as they can provide a more general framework for nonlinear behavior of concrete. Despite its high complexity, it is generally believed that the principal behavior of concrete can be adequately captured by constitutive models based on the plasticity theory (Pekau et al., 1992).

A plasticity model suitable for confined concrete should include pressure dependence, path dependence, non-associative flow rule, work or strain hardening and limited tensile strength features. It has been demonstrated by Karabinis and Rousakis (2002) that the behavior of concrete structural members can be well estimated using a Drucker–Prager (DP) type plasticity model in which parameters related to friction angle and cohesion govern the yielding and hardening criteria, while the parameter related to plastic dilation determines the flow rule.

Extensive research has been conducted on plastic dilation rate in steel confined concrete by Karabinis and Kiousis (1996) and Oh (2002). For FRP confined concrete, relatively few research works have been undertaken. Karabinis et al. (2008), Mirmiran et al. (2000) and Rousakis et al. (2008) adopted a constant plastic dilation rate. However, Yu et al. (2010) showed that plastic dilatation rate varies with plastic strains, as well as lateral stiffness, though without presenting a systematic and explicit model.

In previous studies, the friction angle is assumed to be a material constant irrelevant to hydrostatic stress (Karabinis and Kiousis, 1996; Karabinis and Rousakis, 2002; Karabinis et al., 2008; Mirmiran et al., 2000; Oh, 2002; Richart et al., 1928; Ritchie, 1962; Rousakis et al., 2008; Yu et al., 2010). Therefore the stress path is only governed by the hardening/softening rule that determines the variation of cohesion. However, Vermeer and de Borst (1984) pointed out that concrete's behavior under constant confinement cannot be well modeled by cohesion hardening under a constant friction angle. Therefore, further study of the problem is much needed.

Plastic dilation, friction angle and cohesion for FRP confined concrete (normal-weight) are extensively investigated by analyzing test results, and models for each of them are developed in this paper, leading to a modified DP model for finite element analyses of FRP confined concrete columns.

2. Drucker–prager plasticity model

The DP model was proposed by Drucker and Prager (1952). It can well describe pressure-sensitive materials such as rock, soil and concrete. Similar to other plasticity models, there are three criteria controlling the framework of a DP type model, and hence accuracy of predictions by the model. Numerical studies in this paper are based on the linear extended DP model built in commercial software ABAQUS. Details of the model in the case of uniaxial com-

* Corresponding author. Tel.: +852 34424259; fax: +852 34427612.
E-mail address: yfwu00@cityu.edu.hk (Y.-F. Wu).

0020-7683/$ - see front matter © 2011 Elsevier Ltd. All rights reserved.
doi:10.1016/j.ijsolstr.2011.10.002

pression with uniform confinement are briefly described in the following sections.

2.1. Yielding criterion and hardening/softening rule

The yielding function for the linearly extended DP model is in the form of

$$t - \tan\varphi p - k = 0, \tag{1}$$

where

$$t = f(K)\sqrt{J_2} = f(K)\sqrt{\frac{1}{6}[(\sigma_1-\sigma_2)^2+(\sigma_2-\sigma_3)^2+(\sigma_3-\sigma_1)^2]}, \tag{2}$$

$$p = \frac{-I1}{3} = \frac{-(\sigma_1+\sigma_2+\sigma_3)}{3}, \tag{3}$$

$$f(K) = \frac{\sqrt{3}}{2}\left[1+\frac{1}{K}-\frac{3\sqrt{3}}{2}\left(1-\frac{1}{K}\right)\left(\frac{\sqrt[3]{J_3}}{\sqrt{J_2}}\right)^3\right], \tag{4}$$

where σ_i(i = 1, 2, or 3) is the stress in i direction; k is the hardening/softening parameter, which is the interception of a yielding surface to the t axis (Fig. 1). Its variation governs the development of subsequent yielding surfaces; φ is the friction angle, which reflects the slope of the yield surface in the stress space (Fig. 1). Function $f(K)$ is an indirect expression of Lode's angle combining the second and third invariants of deviatoric stress, J_2 and J_3, respectively. K is a material parameter that accounts for stress-path with the variation of shear strength under a given hydrostatic pressure and determines the shape of the yielding function in the deviatotic plane, ranging from 0.778 to 1. For the case of uniform confinement, $f(K)$ equals to $\sqrt{3}$, irrelevant to K. Here a compression is considered as a negative value and tension positive.

2.2. Flow rule

In the current DP model, plastic potential function G that governs the flow rule is given by,

$$G = t - \tan\beta p + \text{constant}. \tag{5}$$

Increments of the plastic strain can be found by,

$$d\varepsilon_{ij}^p = \lambda\frac{\partial G}{\partial\sigma_{ij}}. \tag{6}$$

In the case of uniformly confined cylinder, $\sigma_1 = \sigma_c$ and $\sigma_2 = \sigma_3 = \sigma_l$, therefore,

$$d\varepsilon_c^p = \lambda\left(\frac{\sqrt{3}}{2\sqrt{\frac{(\sigma_c-\sigma_l)^2}{3}}}\frac{2(\sigma_c-\sigma_l)}{3}+\frac{\tan\beta}{3}\right) = \lambda\left(-1+\frac{\tan\beta}{3}\right), \tag{7}$$

$$d\varepsilon_l^p = \lambda\left(\frac{\sqrt{3}}{2\sqrt{\frac{(\sigma_c-\sigma_l)^2}{3}}}\frac{(\sigma_l-\sigma_c)}{3}+\frac{\tan\beta}{3}\right) = \lambda\left(\frac{1}{2}+\frac{\tan\beta}{3}\right). \tag{8}$$

Plastic strains under monotonic loading can be estimated by deducting elastic strains using isotropic elasticity,

$$\varepsilon_c^p = \varepsilon_c - \frac{1}{E}(\sigma_c - 2\nu\sigma_l), \quad \varepsilon_l^p = \varepsilon_l - \frac{1}{E}[(1-\nu)\sigma_l - \nu\sigma_c]. \tag{9}$$

The following equation can be obtained from Eqs. (7) and (8)

$$\tan\beta = -\frac{3\left(d\varepsilon_c^p + 2d\varepsilon_l^p\right)}{2\left(d\varepsilon_c^p - d\varepsilon_l^p\right)} = -\frac{3d\varepsilon_v^p}{2d\varepsilon_s^p} = \frac{\sqrt{3}}{2}\alpha, \tag{10}$$

where λ is a non-negative scalar parameter; superscript p represents plastic deformation; and E and ν are Young's modulus and Poisson's ratio, respectively. Eq. (10) shows that plastic dilation angle β determines the tangent ratio of plastic volumetric strain ε_v^p, to plastic shear strain ε_s^p, which is of great significance in mathematical modeling of pressure dependent material (Rousakis et al., 2008). Dilation rate α has been adopted in previous studies (Karabinis and Rousakis, 2002; Oh, 2002; Rousakis et al., 2008). Under the current sign regulation, a negative β value indicates a volumetric compaction tendency while a positive value indicates a volumetric expansion tendency. A transition point arises when β is zero in volumetric deformation (Fig. 2).

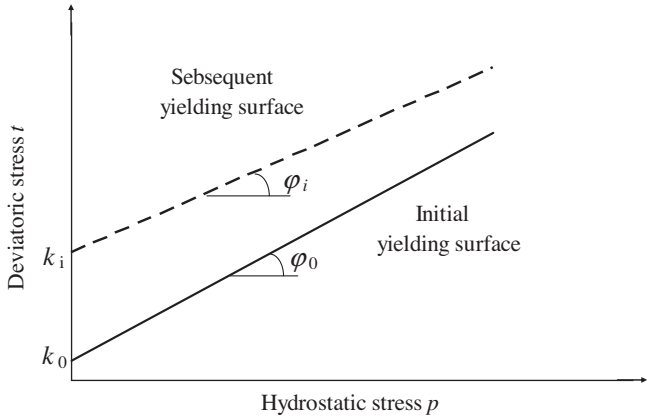

Fig. 1. Yielding surface of Drucker–Prager Model.

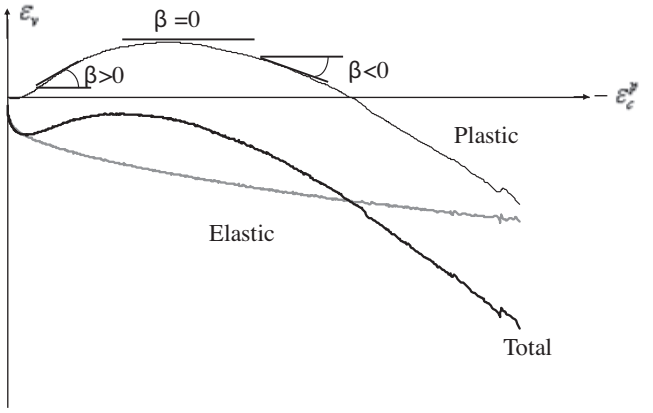

Fig. 2. Total, elastic and plastic volumetric strains.

3. Plastic dilation

3.1. Previous studies

In an FRP confined column, lateral dilation of concrete induces passive confinement from the FRP jacket. Fig. 2 illustrates typical volumetric deformations. As the elastic volumetric deformation is always in compaction and can be calculated accurately, evaluation of the plastic volumetric strain is critical to determination of total volumetric deformation that controls the confinement pressure.

Previous studies on plastic dilation of FRP confined columns were initially based on steel confined cases. Mirmiran et al. (2000) found that a zero plastic dilation rate could give a reasonably close prediction for C29.6 concrete with 6 plies of FRP through a trial-and-error procedure but pointed out that the constant rate could not represent the true dilation tendencies. In an earlier model by Karabinis and Rousakis (2002), an asymptotic function was proposed. Plastic dilation angle β is assumed to decrease from $-27.4°$ ($\alpha = -0.6$) to $-56.3°$ ($\alpha = -\sqrt{3}$) (Fig. 3). The negative β value

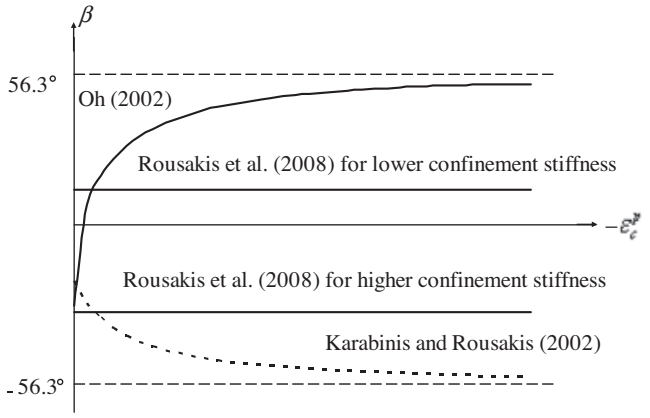

Fig. 3. Existing models for plastic dilation rate, α converted into plastic dilation angle, β.

indicates a plastic volumetric compaction which approaches −56.3° when lateral stiffness of FRP jacket approaches infinity. Oh (2002) proposed another asymptotic function regressed from data generated from empirical models for columns with active confinement. However, its value increases from −40.9° ($\alpha = -0.866$) to 56.3° ($\alpha = \sqrt{3}$) (Fig. 3). Rousakis et al. (2008) later considered a constant dilation rate that depends on unconfined concrete strength and the modulus of confinement. However, it is inconsistent with the observation that the slope of plastic potential function should vary with the increasing lateral stress (Grassl et al., 2002; Han and Chen, 1985; Imran and Pantazopoulou, 2001; Papanikolaou and Kappos, 2007; Smith et al., 1989). Yu et al. (2010) demonstrated that the flow rule can properly reflect the effect of plastic deformation and the rate of confinement increment can lead to a reasonably close prediction of behavior of FRP confined concrete. They presented a procedure for obtaining variations of the potential function parameter; however, no explicit model has been provided.

3.2. Test observation and analytical modeling

The test data collected for this analytical study include 6 FRP confined column specimens (diameter $D = 152$ mm and height $H = 305$ mm) tested by Teng et al. (2007b) and 23 FRP confined specimens (diameter $D = 152$ mm and height $H = 305$ mm) tested by Jiang and Teng (2007). Unconfined concrete strength varies from 33.1 MPa to 47.6 MPa (Table 1). From the test data, β is calculated using Eq. (10), where elastic modulus E is calculated in accordance with ACI 318 (Eq. (11)) and v is set as 0.2,

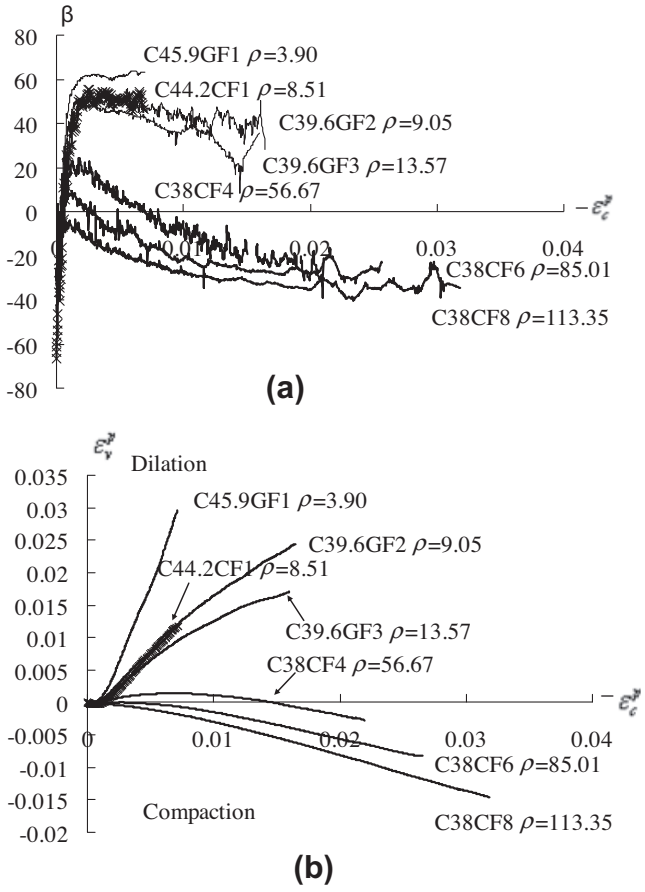

Fig. 4. Test results for plastic dilation: (a) plastic dilation angel, β, (b) plastic volumetric strain.

$$E_c = 4734\sqrt{f'_c}. \tag{11}$$

Fig. 4 shows a series of such curves and the corresponding plastic volumetric deformation curves with different lateral stiffnesses of FRP and unconfined concrete strength. Plastic dilation angle β in Fig. 4a is clearly very different from Fig. 3. A similar trend is observed in all curves that relate β with axial plastic strain, as illustrated by the typical curve in Fig. 5, where β begins from a negative value β_0, and increases to the maximum point $(\varepsilon^p_{cr}, \beta_m)$. Afterwards, it decreases to an asymptotic value β_u. The comparison in Fig. 4a shows that the curve moves downward with increase in lateral stiffness ratio ρ, defined by Eq. (12),

Table 1
Specimens properties.

Source	ID	Number	D (mm)	H (mm)	f'_c (MPa)	Fiber type	t_f(mm)	E_f(GPa)	ρ	R^2 (β curve)
Teng et al. (2007b)	C39.6GF1	2	152	305	39.6	Glass	0.17	80.1	4.52	0.9647
	C39.6GF2	2	152	305	39.6	Glass	0.34	80.1	9.05	0.7963
	C39.6GF3	2	152	305	39.6	Glass	0.51	80.1	13.57	0.7825
Jiang and Teng, 2007	C33.1GF1	2	152	305	33.1	Glass	0.17	80.1	5.41	0.9822
	C45.9GF1	2	152	305	45.9	Glass	0.17	80.1	3.90	0.9087
	C45.9GF2	2	152	305	45.9	Glass	0.34	80.1	7.81	0.8745
	C45.9GF3	2	152	305	45.9	Glass	0.51	80.1	11.71	0.8038
	C38CF4	2	152	305	38	Carbon	0.68	240.7	56.67	0.8043
	C38CF6	2	152	305	38	Carbon	1.02	240.7	85.01	0.7951
	C38CF8	2	152	305	38	Carbon	1.36	240.7	113.35	0.9165
	C37.7CF1	2	152	305	37.7	Carbon	0.11	260	9.98	0.8924
	C44.2CF1	2	152	305	44.2	Carbon	0.11	260	8.51	0.9593
	C44.2CF2	2	152	305	44.2	Carbon	0.22	260	17.03	0.9123
	C47.6CF3	3	152	305	47.6	Carbon	0.33	250.5	22.85	0.9134

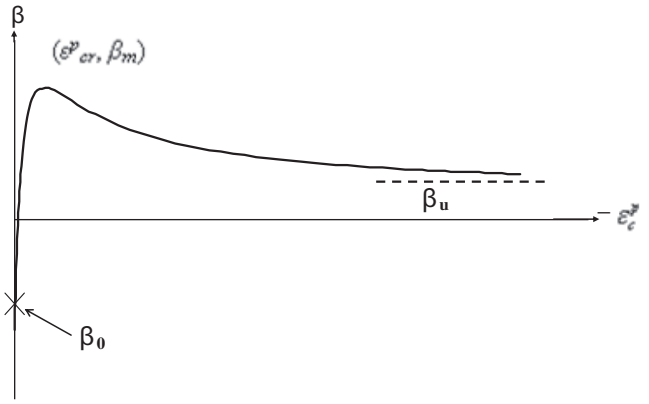

Fig. 5. Typical dilation curve.

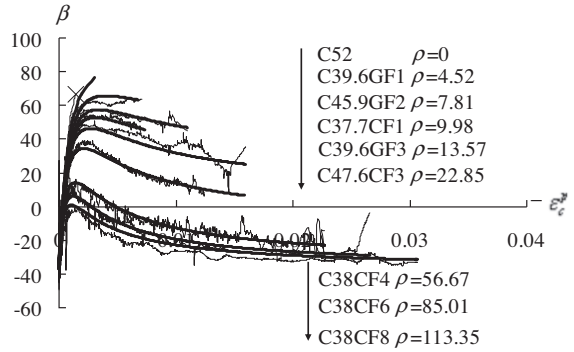

Note: all specimens are from Table 1 except C52 that is from Wang and Wu (2008).

Fig. 6. Performance of plastic dilation model.

$$\rho = \frac{2E_f t_f}{Df'_c}, \tag{12}$$

where E_f and t_f are elastic modulus and thickness of FRP, respectively; D is the diameter of the column; and f'_c is the unconfined concrete strength. For curves with different FRP stiffnesses and unconfined concrete strengths but with a similar value of ρ, the β curve and the ε^p_v curve are similar, as shown by specimens C39.6GF2 and C44.2CF1 in Fig. 4. Therefore, it can be concluded that ρ is the governing factor (at least the dominant factor) that affects the curve of β; hence it will be sufficiently accurate for engineering use to assume that β curve is only affected by ρ. In fact, this assumption is consistent with the conclusion by Yu et al. (2010) that stiffness of the FRP jacket affects the plastic dilation angle.

The typical plastic dilation curve in Fig. 4 can be well represented by the following equation:

$$\beta = \frac{A + B\varepsilon^p_c + C(\varepsilon^p_c)^2}{1 + D\varepsilon^p_c + E(\varepsilon^p_c)^2}, \tag{13a}$$

which is illustrated by the general shape in Fig. 5. Using the boundary values, Eq. (13)a can be more conveniently expressed as

$$\beta = \frac{\beta_0 + (M_0 + \lambda_1\beta_0)\varepsilon^p_c + \lambda_2\beta_u(\varepsilon^p_c)^2}{1 + \lambda_1\varepsilon^p_c + \lambda_2(\varepsilon^p_c)^2}. \tag{13}$$

The three coefficients λ_1, λ_2 and β_u are functions of ρ. β_0 and M_0 are the initial value and the corresponding slope of β curve at $\varepsilon^p_c = 0$, which are generally found to be constants from test curves, given by

$$\beta_0 = -37, \quad M_0 = \left.\frac{d\beta(\varepsilon^p_c)}{d\varepsilon^p_c}\right|_{\varepsilon^p_c=0} = 157000. \tag{14}$$

Eq. (14) is conceptually reasonable as stiffness of confinement does not affect initial plastic dilation properties (Handin, 1969; Rousakis et al., 2008). By best matching all test curves of β to Eq. (13), the other three coefficients, λ_1, λ_2 and β_u, are regressed to be

$$\lambda_1 = 11.61\rho + 980, \tag{15}$$

$$\lambda_2 = 5700\rho + 225000, \tag{16}$$

$$\beta_u = 101.66\exp(-0.06\rho) - 37.5. \tag{17}$$

Fig. 6 shows comparison between the proposed model and test curves of β, which shows a reasonable agreement. The correlation coefficients between them are listed in Table 1.

3.3. Sensitivity study

As constant β value was adopted in previous studies by many researchers (Karabinis et al., 2008; Mirmiran et al., 2000; Rousakis et al., 2008), there is a possibility that the stress–strain response is insensitive to the plastic dilation curve. Therefore, a sensitivity study was undertaken to find out how sensitive parameters β_0, M_0, β_m and β_u (see Fig. 5) are to the stress–strain curve. The reference specimen is a C39.6 cylinder with 2 layers of glass FRP (Teng et al., 2007b). Values of the four parameters are calculated to be $\beta_0 = -50.86°$, $M_0 = 125863°$, $\beta_m = 52.6°$, and $\beta_u = 35.4°$, obtained by regressing the test dilation curve to the model curve in Fig. 5. With a 50% deviation from values of β_0 and M_0, the maximum difference in axial strain at FRP rupture is 2.3% and 2.4%, respectively; see Fig. 7(a). Therefore, average test results for β_0 and M_0 are used as constants for these two parameters in Eq. (14). However, a 20%

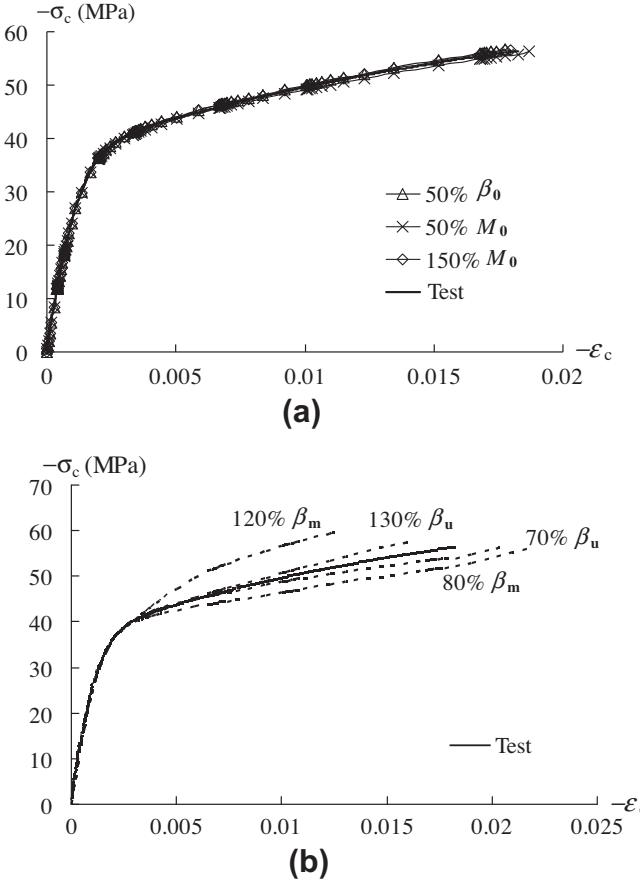

Fig. 7. Sensitivity study of dilation parameters: (a) initial modulus M_0 and initial plastic dilation angle β, (b) maximum and ultimate plastic dilation angle β_m, β_u.

deviation for β_m induces over 30% difference in the axial strain; and a 30% deviation for β_u causes 12% difference in the axial strain, as illustrated in Fig. 7(b). Therefore, the stress–strain response is sensitive to β_m and β_u but insensitive to variations of β_0 and M_0. The theoretical stress–strain curves in Fig. 7 are given by the finite element model presented in Section 5 with the plastic dilation model given by Eq. (13) and the friction and cohesion models proposed in Section 4.

3.4. Discussions

On being subjected to uniaxial compressive loading, both the concrete core and the FRP jacket expand laterally at a similar rate in the beginning due to the similar Poisson's ratios of the two materials. The concrete core exhibits larger lateral dilation than FRP afterwards, when significant microcracking occurs in the concrete. The confinement does not take effect until the lateral-to-axial strain ratio of the concrete exceeds the Poisson's ratio of the FRP jacket. Therefore, β takes an initial negative value β_0 (volumetric contraction), irrelevant to the lateral stiffness ratio of FRP. When the axial load further increases, microcracking develops quickly in concrete and hence β increases quickly. During this stage the passive confinement from FRP takes effect, which counteracts concrete's lateral expansion and leads to a reduced rate of increase in β, as reflected by the ascending part of the curve in Fig. 5. During the dilation of concrete, the passive confinement from FRP increases continuously, which reduces the dilation rate of concrete such that β reaches its peak β_m and starts to drop. When the interaction between the jacket and the concrete is stabilized, β reaches an asymptotic value, β_u.

It is obvious that the higher the lateral stiffness is, the larger is the constraint FRP can exert. As a result, an increase in the lateral stiffness ratio decreases values of β_m and β_u, as correctly reflected by Eq. (13). Clearly, a relatively stiffer jacket or a larger ρ mobilizes the confinement faster and hence causes an earlier onset of the peak point or the reduction of the ε_{cr}^p value, which is also the case for Eq. (13). Naturally, ε_{cr}^p, β_m and β_u approach a lower bound when ρ approaches infinity, because at a sufficiently high confinement a further increase in stiffness of the FRP jacket cannot further restrain the lateral expansion to a smaller rate than the Poisson's ratio of FRP.

Performance of the proposed model (Eq. (13)) is depicted in Fig. 8 for two typical cases, one with low and other with high jacket stiffness. It can be seen from the test results in Fig. 8 that the case with the thin FRP jacket exhibits a monotonic plastic volumetric expansion until FRP rupture, while the case with the thick jacket shows significant plastic volumetric contraction after the initial expansion at low confinement stress. For comparison, the three existing models are also shown together in the figure. Clearly, only the proposed model correctly describes dilation characteristics of FRP confined concrete.

FRP confined concrete exhibits different volumetric plastic deformation patterns at different lateral stiffness ratios (Fig. 4b). Such variations can be well captured by the proposed model comprehensively but not by any of the existing models. The asymptotic model of Oh (2002) overestimates the confinement effect in the beginning and underestimates it near the end for cases with higher confinement stiffness, and is suitable only for concrete under constant confinement which takes effect earlier than the passive one, as shown in Fig. 8. The Karabinis and Rousakis (2002) model only describes plastic volumetric contraction without considering jacket stiffness, and hence, is only suitable for highly confined concrete. Although (Rousakis et al., 2008) considered stiffness of confinement, the constant value of plastic dilation rate determines the linear relationship between ε_v^p and ε_c^p. Therefore, it fails to capture the nonlinear development.

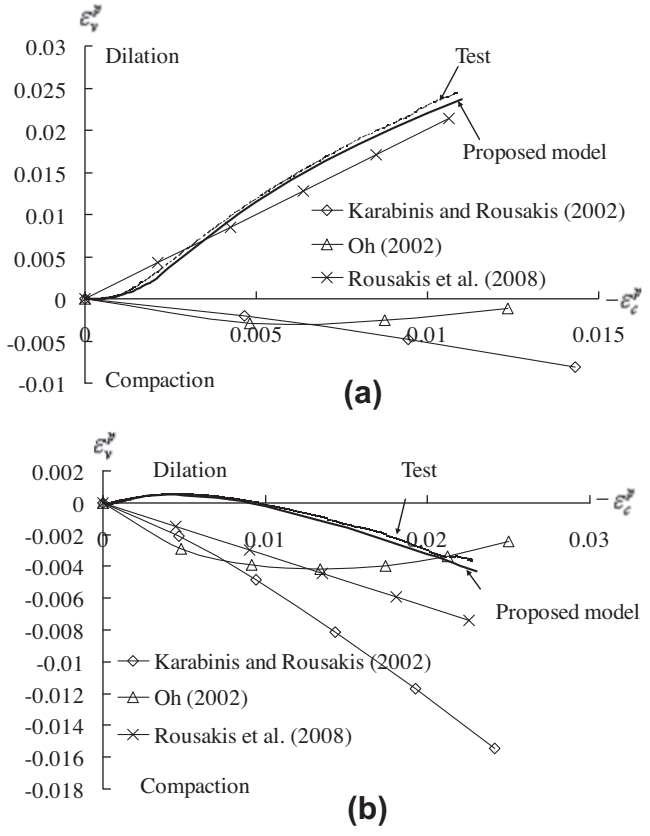

Fig. 8. Comparison between different dilation models: (a) ρ = 7.81, (b) ρ = 56.67.

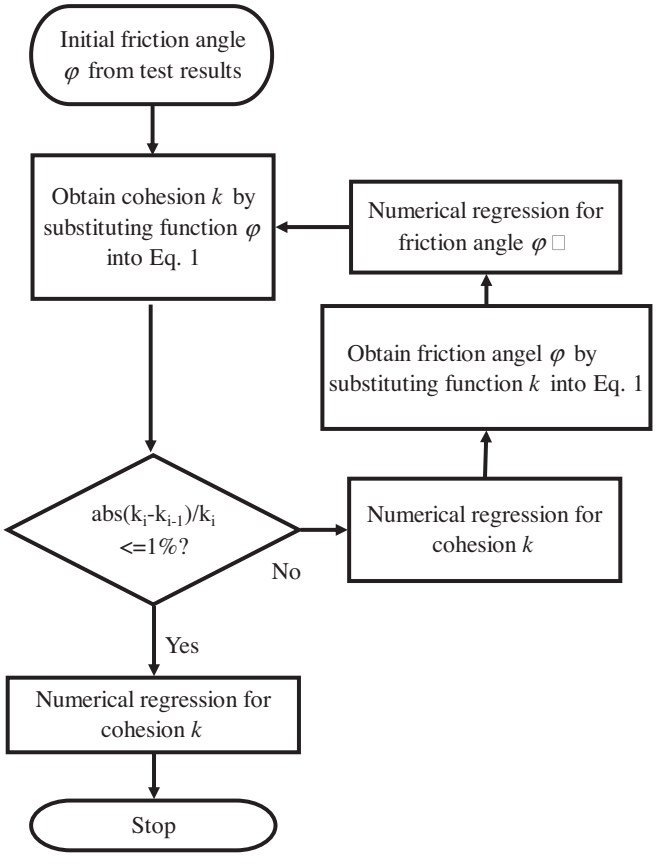

Fig. 9. Iteration flow chart.

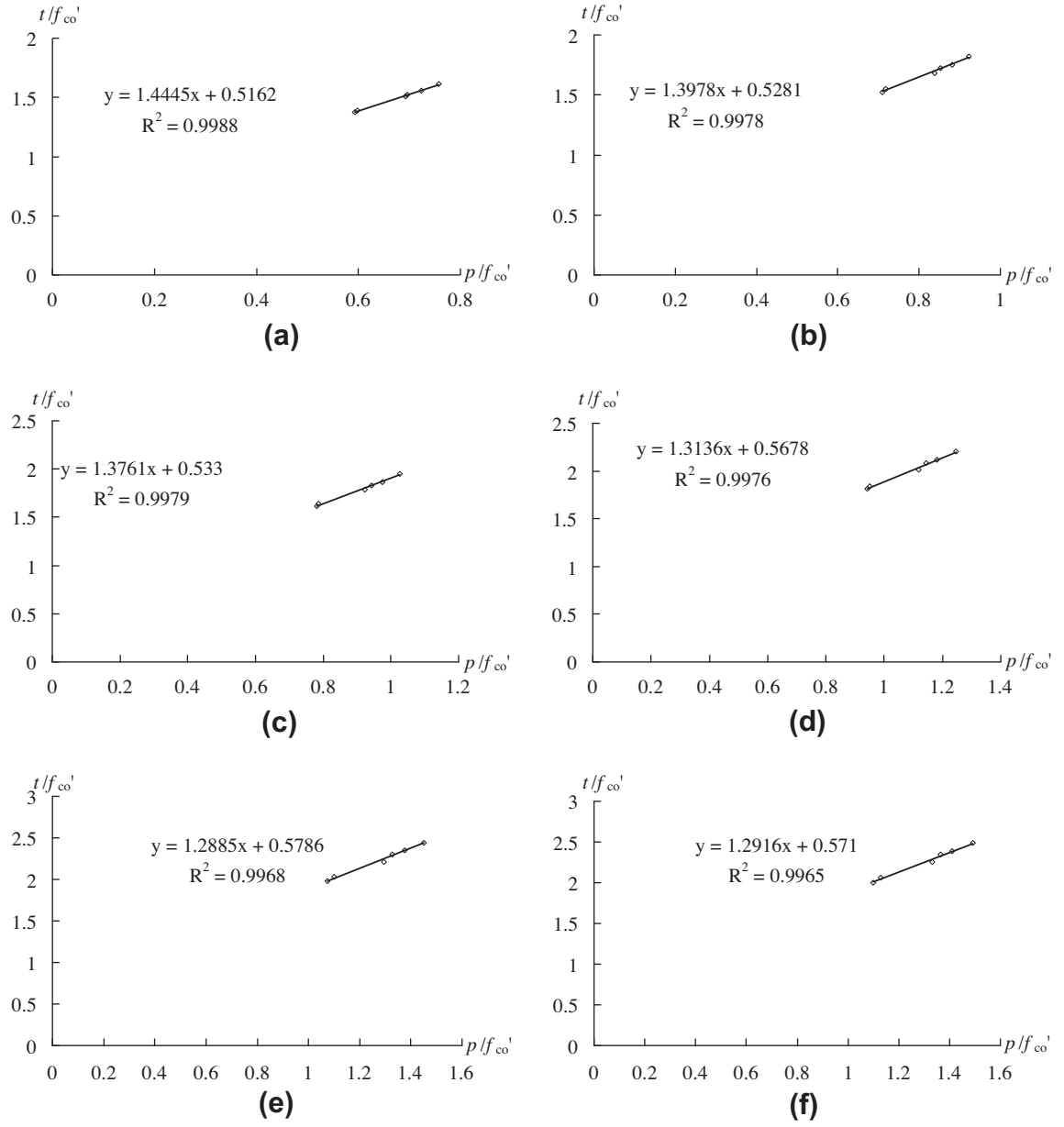

Fig. 10. Friction angle at different equivalent plastic strains: (a) $\tilde{\varepsilon}_p = 0.005$, (b) $\tilde{\varepsilon}_p = 0.008$, (c) $\tilde{\varepsilon}_p = 0.01$, (d) $\tilde{\varepsilon}_p = 0.015$, (e) $\tilde{\varepsilon}_p = 0.02$, (f) $\tilde{\varepsilon}_p = 0.021$.

4. Friction and cohesion

4.1. Previous studies on friction angle φ

Friction angle φ in Eq. (1) can be converted through Eq. (18) to an internal friction angle ϕ defined in the Mohr–Coulomb theory when DP yielding cone circumscribes the Mohr–Coulomb hexagonal pyramid (Karabinis and Kiousis, 1996; Karabinis and Rousakis, 2002; Karabinis et al., 2008; Mirmiran et al., 2000; Oh, 2002; Richart et al., 1928; Ritchie, 1962; Rousakis et al., 2008; Yu et al., 2010):

$$\tan\varphi = \frac{6\sin\phi}{3-\sin\phi}. \tag{18}$$

The internal friction angle is obtained by drawing a tangent line to a series of Mohr–Coulomb circles in the state of failure in triaxial experimental tests of concrete. The failure state is defined as the point where the concrete reaches a defined failure status such as the onset of the peak strength or a certain axial strain. The internal friction angle is usually regarded as a material constant related to concrete strength but irrelevant to loading history (Richart et al., 1928; Ritchie, 1962). However, Vermeer and de Borst (1984) pointed out that the concrete behavior cannot be well fitted by cohesion hardening/softening under constant friction angle, as it results in concrete initial yielding point of deviatoric stress ($\sigma_c - \sigma_l$), increasing with the increase in constant lateral confinement, which is not in line with mechanical behavior of concrete. As the Mohr–Coulomb theory is for describing the behavior of brittle materials, and for rocks and concrete, when the brittleness reduces and the softness increases under increasing deformation, it is possible that the angle of internal friction reduces with the reduction in brittleness of the material (Handin, 1969).

The above discussion shows that a good understanding and common conclusion on the internal friction angle of confined concrete is yet to be reached. The following study tries to look at the

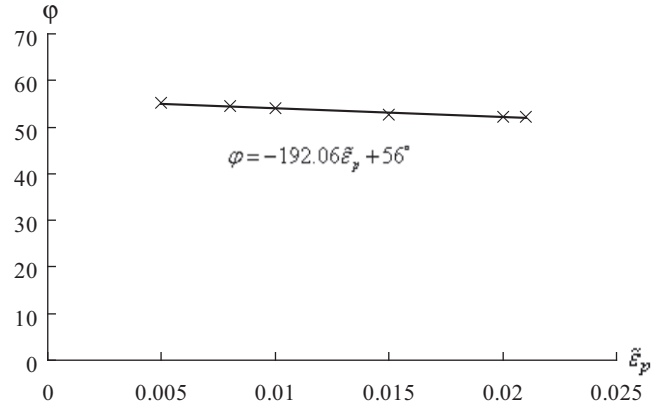

Fig. 11. Variation of friction angle.

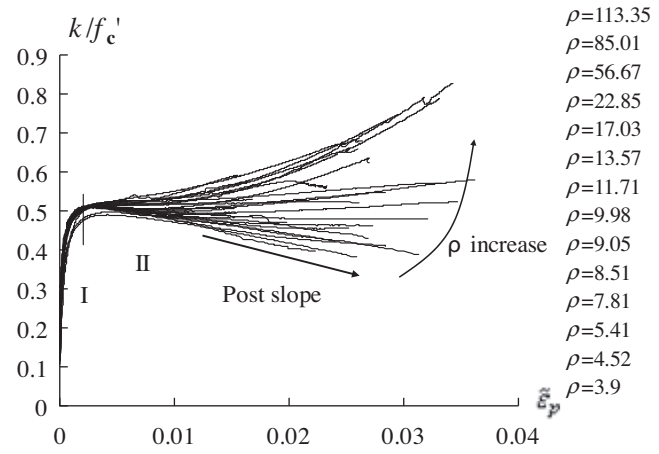

Fig. 12. Normalized cohesion vs. equivalent plastic strain.

problem from another angle by investigating variations of friction parameters under different equivalent plastic strains based on experimental results, showing that the frictional coefficient changes when the material deforms.

4.2. Previous studies on hardening–softening function k

In the framework of DP type constitutive relationship, k is the hardening/softening function which governs the development of the subsequent yielding surface. Since this is the deviatoric stress t at zero hydrostatic pressure p, it is the cohesive shear resistance. Many researchers believe that the variation of cohesion k is highly related to plastic deformation and confinement level. Based on actively confined concrete, Karabinis and Kiousis (1996) and Oh (2002) proposed a hardening–softening model determined by plastic strains and confinement level, with 8 and 13 parameters, respectively. Yu et al. (2010) proposed a procedure for calculating k based on plastic strain and confinement value, using Teng et al., 2007a empirical stress–strain model. It is assumed in all previous studies that cohesion k in FRP confined concrete is the same as in actively confined concrete under the same confinement pressure. This assumption causes inaccuracy in modeling. Meanwhile, these hardening–softening functions are based on the assumption that frictional resistance ($\tan\varphi$) is constant throughout the loading process.

4.3. Test observation and analytical modeling

As cohesion and friction angle are tied up through Eq. (1), an iteration procedure is used to separate them and derive friction angle φ and cohesion k from test data. The iteration procedure is illustrated in Fig. 9.

4.3.1. Initial value for iteration

There are only three possible factors that may affect internal shear resistance (including cohesion and frictional coefficient): concrete type (represented by unconfined concrete strength f_c'), state of internal damage (characterized by the equivalent principal plastic strain $\tilde{\varepsilon}_p$), and confinement stiffness (described by ρ). To isolate factor $\tilde{\varepsilon}_p$ from the other two factors f_c' and ρ, six specimens (Table 1) of concrete grade C38 and lateral confinement ratios of 56.67, 85.01 and 113.35 are selected. Although values of ρ are not equal for these six specimens, these confinement ratios are sufficiently high and, therefore, that does not cause large variations in dilation properties of these specimens (the variation is addressed later, through iteration). Therefore, it is assumed that the cohesion is the same in these specimens when $\tilde{\varepsilon}_p$ takes the same value; the friction angle can be calculated through the following process:

a. for a particular axial loading on a specimen, calculate deviatoric stress $t = \sqrt{3J_2}$, and mean stress $p = -I_1/3$. The lateral (confinement) stress is calculated using the measured FRP lateral strain.
b. calculate the corresponding axial and lateral plastic strains through Eq. (9). The elastic modulus, E, is calculated with Eq. (11), and the Poisson's ratio, ν, is set to be 0.2.
c. calculate the equivalent principal plastic strain by

$$\tilde{\varepsilon}_p = \int \sqrt{d\varepsilon_i^p \cdot d\varepsilon_i^p}; \tag{19}$$

d. repeat Steps a to c for all axial loading values recorded for one test specimen;
e. repeat Steps a to d for all test specimens, and plot the deviatoric stress and mean stress of the specimens in p-t coordinates under the same equivalent principal plastic strain in Fig. 10. The points in one figure (for one value of equivalent principal plastic strain) are calculated from different specimens, instead of one specimen; and
f. the friction angle is the slope of the lines in Fig. 10. By plotting the friction angle and its corresponding plastic strain from one figure as one point in Fig. 11, a series of points are produced and shown in Fig. 11.

Clearly, a straight line relating $\tilde{\varepsilon}_p$ and φ is obtained in Fig. 11 and given by Eq. (20).

Table 2
Parameters in each iteration.

Iteration	φ_0	κ	E_p	η	a_1	a_2	a_3	b_1	b_2	b_3
1st	56.00	−192.06	2700	6400	0.13	0.0046	−0.025	−2.93	−15.99	0.21
2nd	56.20	−209.24	2700	6472	0.12	0.0044	−0.022	−2.10	−25.43	1.13
3rd	56.32	−219.70	2700	6472	0.12	0.0044	−0.022	−1.32	−32.99	1.59
4th	56.44	−226.00	2700	6587	0.12	0.0044	−0.023	−0.75	−41.06	2.52

$$\varphi = \varphi_0 + \kappa \cdot \tilde{\varepsilon}_p. \tag{20}$$

The suitability of Eq. (20) is further discussed in Section 4.3.3.

4.3.2. Cohesion model

Assuming the friction angle model of Eq. (20) is applicable to all specimens in Table 1, values of cohesion are calculated using Eq. (1) (Fig. 12). The typical relationship between normalized cohesion k/f_c' and $\tilde{\varepsilon}_p$ can be well modeled by the following equation:

$$\frac{k(\tilde{\varepsilon}_p, \rho)}{f_c'} = k_0 + E_P \frac{\tilde{\varepsilon}_p}{1 + \eta \cdot \tilde{\varepsilon}_p} + p_1(\rho)\tilde{\varepsilon}_p^2 + p_2(\rho) \cdot \tilde{\varepsilon}_p, \tag{21}$$

where k_0 equals to 1/8, supposing the initial yielding stress is 1/4 of unconfined concrete strength ($p = \sigma_c - 2\sigma_l = 0\sigma_l = 0.5\sigma_c, k = t = (\sigma_c - \sigma_l) = 0.5\sigma_c k/f_c' = 1/8$ when $\sigma_c = f_c'/4$), and E_p is the initial slope of the cohesion curve. η is a constant parameter. Coefficients p_1 and p_2 are functions of ρ and can be determined by the following equations:

$$p_1 = \frac{\rho}{a_1 + a_2\rho + a_3\sqrt{\rho}}, \tag{22}$$

$$p_2 = \frac{b_1\rho + b_2}{\rho + b_3}. \tag{23}$$

4.3.3. Results

After obtaining the initial models of Eqs. (20) and (21), the iteration process shown in Fig. 9 is used to calculate the coefficients in these two equations. The iteration process and the final results are listed in Table 2. Convergence is considered reached after the 4th iteration when $max|k_i - k_{i-1}|/k_i < 1\%$ between the two adjacent iterations.

The cohesion model (Eq. (21)) involves all the three factors. However, the friction model (Eq. (20)) only involves the equivalent plastic strain. By substituting Eq. (21) into Eq. (1), friction angles φ are calculated for all specimens, shown in Fig. 13 by thin lines. The thick solid line in the figure gives the friction model. If the thin lines and the solid line completely match, it means both Eqs. (20) and (21) perfectly match all results and the proposed models have a zero scatter of results. For heterogeneous materials like concrete, this is impossible. The maximum scattering between the dotted lines and the solid line is 5.4%, which is considered well within the acceptable range of error for experimental test results.

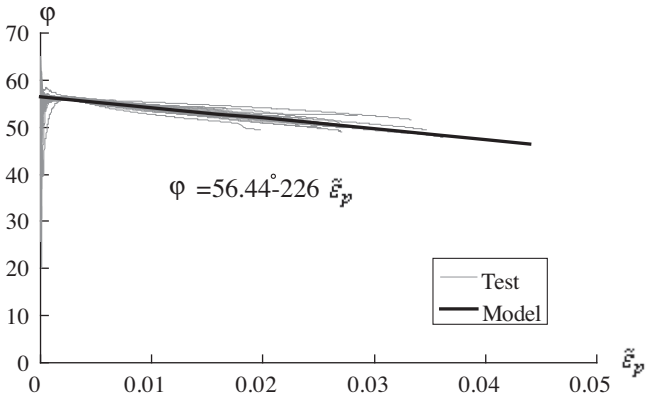

Fig. 13. Performance of the friction model.

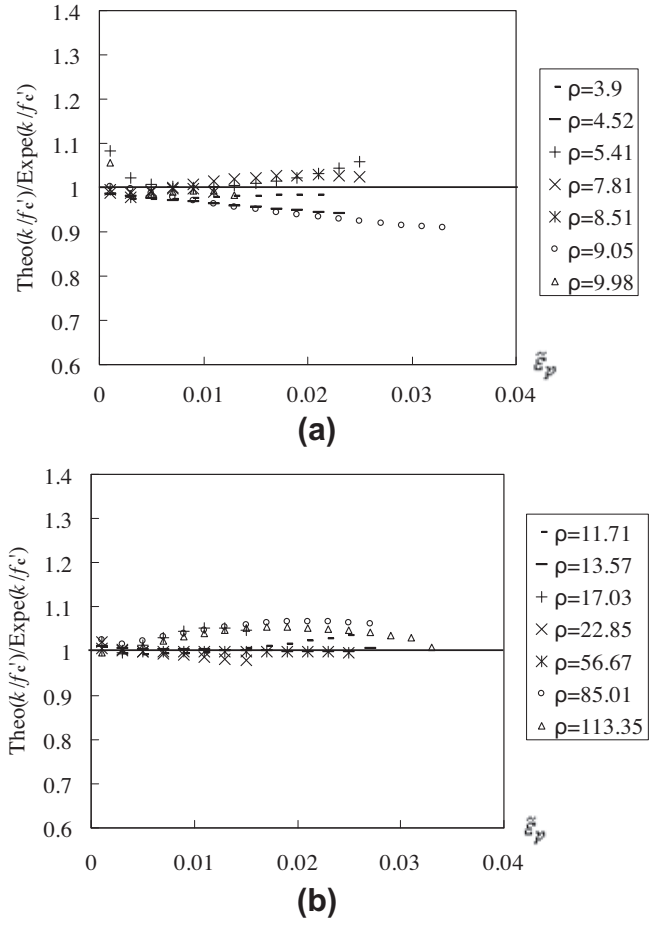

Fig. 14. Theoretical value of cohesion compared with experimental results.

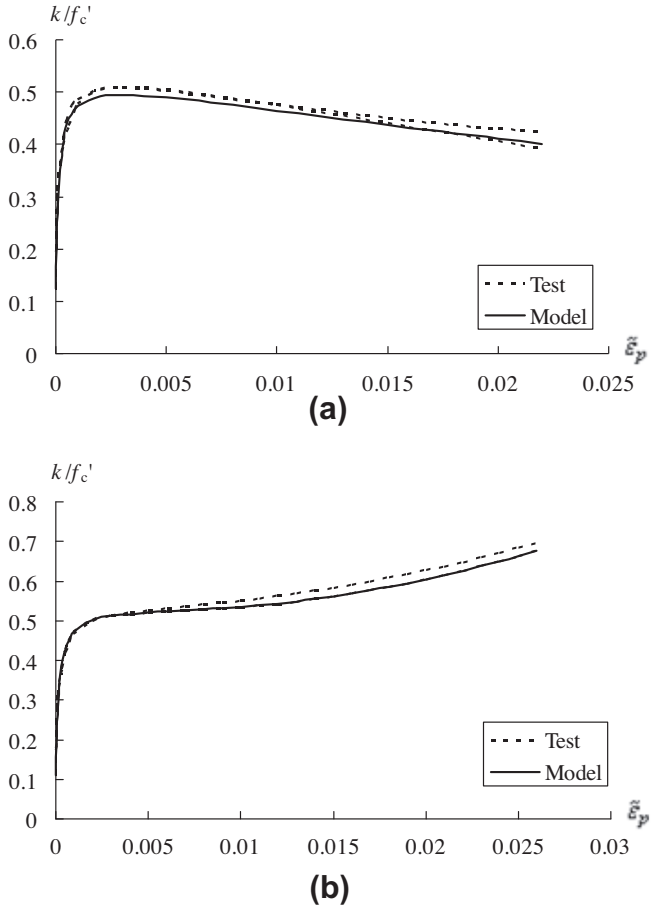

Fig. 15. Performance of the cohesion model: (a) ρ = 3.9, (b) ρ = 56.67.

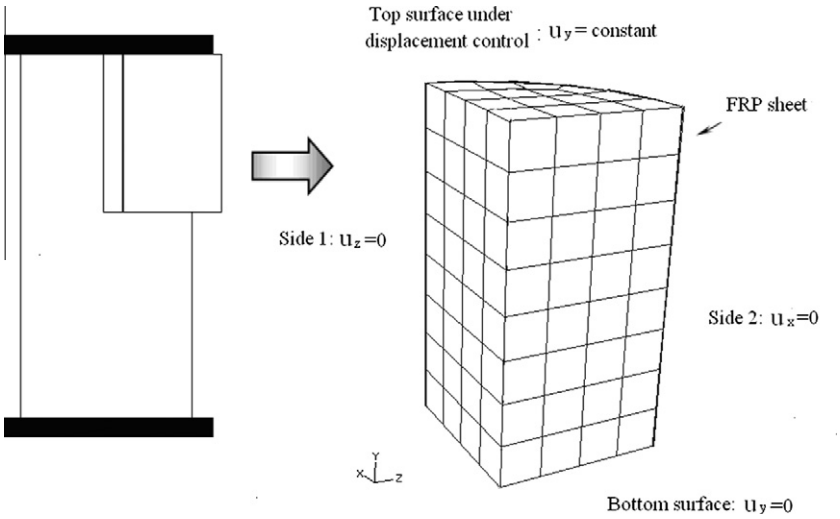

Fig. 16. Column model.

Table 3
Comparison of simulation and test results.

Source	ID	No.	f'_c (MPa)	Fiber type	ρ	ε_{cu}(Test) (%)	ε_{cu} (FEA) (%)	Error	f'_{cc} (Test) (MPa)	f'_{cc} (FEA) (MPa)	Error
Teng et al. (2007b)	C39.6GF1	2	39.6	Glass	4.52	0.298	0.334	12.11%	41.2	39.7	3.52%
	C39.6GF2	2	39.6	Glass	9.05	1.977	1.717	13.15%	55.5	54.1	2.43%
	C39.6GF3	2	39.6	Glass	13.57	2.175	2.129	2.11%	63.3	65.8	3.95%
Jiang and Teng (2007)	C33.1GF1	2	33.1	Glass	5.41	1.285	0.907	29.43%	42.0	33.5	20.24%
	C45.9GF1	2	45.9	Glass	3.9	0.298	0.334	12.11%	47.2	45.7	3.18%
	C45.9GF2	2	45.9	Glass	7.81	1.227	1.229	0.16%	54.0	56.0	3.70%
	C45.9GF3	2	45.9	Glass	11.71	1.729	1.842	6.53%	65.3	69.8	6.93%
	C38CF4	2	38	Carbon	56.67	2.582	2.639	2.21%	108.8	110.4	1.52%
	C38CF6	2	38	Carbon	85.01	2.938	2.972	1.15%	132.4	137.3	3.74%
	C38CF8	2	38	Carbon	113.35	3.622	3.204	11.53%	159.9	163.6	2.31%
	C37.7CF1	2	37.7	Carbon	9.98	0.905	0.899	0.64%	49.4	46.6	5.67%
	C44.2CF1	2	44.2	Carbon	8.51	0.789	0.712	9.80%	49.6	50.6	2.02%
	C44.2CF2	2	44.2	Carbon	17.03	1.165	1.384	18.84%	64.3	68.4	6.38%
	C47.6CF3	3	47.6	Carbon	22.85	1.687	1.647	2.37%	84.6	84.4	0.20%
Lam and Teng (2004)	C35.9CF1	3	35.9	Carbon	15.15	1.224	1.110	9.31%	50.3	51.4	2.25%
	C35.9CF2	3	35.9	Carbon	30.3	1.832	1.829	0.16%	70.1	72.4	3.33%
	C34.3CF3	3	34.3	Carbon	47.57	2.326	2.111	9.24%	90.1	84.1	6.67%
	C38.5GF1	2	38.5	Glass	9.46	1.387	1.410	1.66%	55.1	50.9	7.62%
	C38.5GF2	2	38.5	Glass	18.92	2.322	2.582	11.20%	76.5	77.5	1.31%
Lam et al. (2006)	C41.1CF1	3	41.1	Carbon	13.21	1.07	1.071	0.09%	55.0	56.4	2.55%
	C38.9CF2	3	38.9	Carbon	27.57	1.747	1.756	0.52%	73.9	73.5	0.54%
Matthys et al. (1999)	C34.9CF1	2	34.9	Carbon	11.00	0.785	0.883	12.54%	43.3	41.5	4.01%
	C34.9CF2	2	34.9	Carbon	58.68	0.380	0.452	18.90%	41.0	49.8	21.35%
Bullo (2003)	C32.54CF1	3	32.54	Carbon	27.17	0.863	0.766	11.33%	56.8	47.6	16.19%
	C32.54CF3	3	32.54	Carbon	79.90	1.593	1.493	6.28%	93.7	82.2	12.28%
Cui (2009)	C48.1GF1	2	48.1	Carbon	23.25	1.520	1.774	16.69%	83.8	87.9	4.95%
	C48.1GF2	2	48.1	Carbon	46.50	2.335	2.773	18.76%	118.1	131.1	11.10%
	C48.1GF3	2	48.1	Carbon	69.76	2.945	3.481	18.20%	158.2	171.7	8.58%
	C45.6CF1	2	45.6	Carbon	7.65	1.260	1.147	8.94%	56.6	54.4	3.72%
	C45.6CF2	2	45.6	Carbon	15.30	2.055	2.197	6.92%	82.4	79.1	3.98%
	C45.6CF3	2	45.6	Carbon	22.95	2.865	3.150	9.96%	106.3	106.0	0.25%
	C45.7CF1	2	45.7	Carbon	20.09	1.070	1.111	3.84%	65.8	69.3	5.35%
	C45.7CF2	2	45.7	Carbon	41.43	1.280	1.345	5.11%	83.7	88.7	6.00%
	C45.7CF3	2	45.7	Carbon	61.51	1.495	1.467	1.86%	97.3	103.6	6.49%
Wang and Wu (2008)	C31.4CF1	3	31.4	Carbon	15.34	1.476	1.230	16.65%	49.7	46.2	7.11%
	C31.4CF2	3	31.4	Carbon	30.69	2.152	2.350	9.22%	67.8	69.9	3.10%
	C52.05CF1	3	52.05	Carbon	9.55	1.035	1.332	28.74%	66.0	67.8	2.71%
	C52.05CF2	3	52.05	Carbon	19.10	1.912	2.230	16.65%	95.1	96.8	1.83%

Note: f'_{cc} and ε_{cu} are the maximum axial stress and corresponding axial strain, respectively.

Fig. 14 shows the error of the proposed model in another way. By substituting Eq. (20) into Eq. (1), test result of cohesion k can be calculated for all specimens and compared with the theoretical prediction given by Eq. (21). The errors in Fig. 14 again show that the theoretical value (Theo $(k/f_c)'$) is within 10% of experimental result (Expe $(k/f_c)'$) for all specimens at any plastic strain value, which is considered very good for materials like concrete. Therefore, the proposed models are acceptable. Fig. 15a and b further

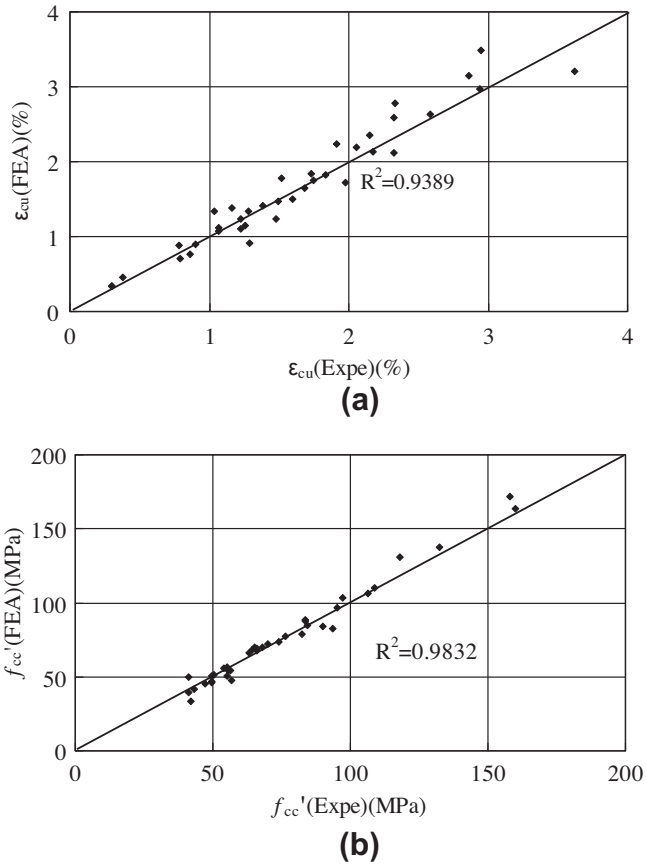

Fig. 17. Comparison of ultimate axial strain and strength: (a) ultimate axial strain, (b) ultimate axial stress.

display the full curve of cohesion for two typical cases, one with low confinement ratio and the other with high confinement ratio; both show a very good match to the test results.

4.4. Discussion

A plastic slip constitutes an irrevocable relocation of particles in a microscopic sense. Parameter tan φ can be seen as the kinetic frictional coefficient contributing to the resistance to plastic slip. In view of plastic damage, the wear during continuous plastic slipping induces looser granular, which weakens the frictional resistance. Therefore, the friction angle decreases when plastic strain increases. Eq. (20) correctly reflects this trend.

In the case of unconfined concrete, the following lateral-to-axial strain model is adopted by Teng et al. (2007a):

$$\frac{\varepsilon_c}{\varepsilon_{cc}} = 0.85\left\{\left[1+0.75\left(-\frac{\varepsilon_l}{\varepsilon_{cc}}\right)\right]^{0.7} - \exp\left[7\left(-\frac{\varepsilon_l}{\varepsilon_{cc}}\right)\right]\right\}, \tag{24}$$

$$\varepsilon_{cc} = 0.000937\sqrt[4]{f_c'}. \tag{25}$$

in which ε_c and ε_l are axial and lateral strains, respectively, and $\varepsilon_{cc}$is unconfined axial strain corresponding to the unconfined concrete strength f_c' given by Popovics (1973). The friction angle φ at peak strength can be obtained through Eq. (20) based on Eqs. (24), (25). The corresponding internal frictional angle ϕ can then be obtained from Eq. (18) to give:

$$\phi = 36.65^\circ - 1.1^\circ\left(\frac{f_c'}{1000}\right). \tag{26}$$

The above derived result from the proposed models is in line with experimental observations by Dahl (1992) and Mahboubi and Ajorloo (2005) in that the internal friction angle slightly decreases with increase in concrete strength, and its value is close to the typical value of about 37°. (Richart et al., 1928).

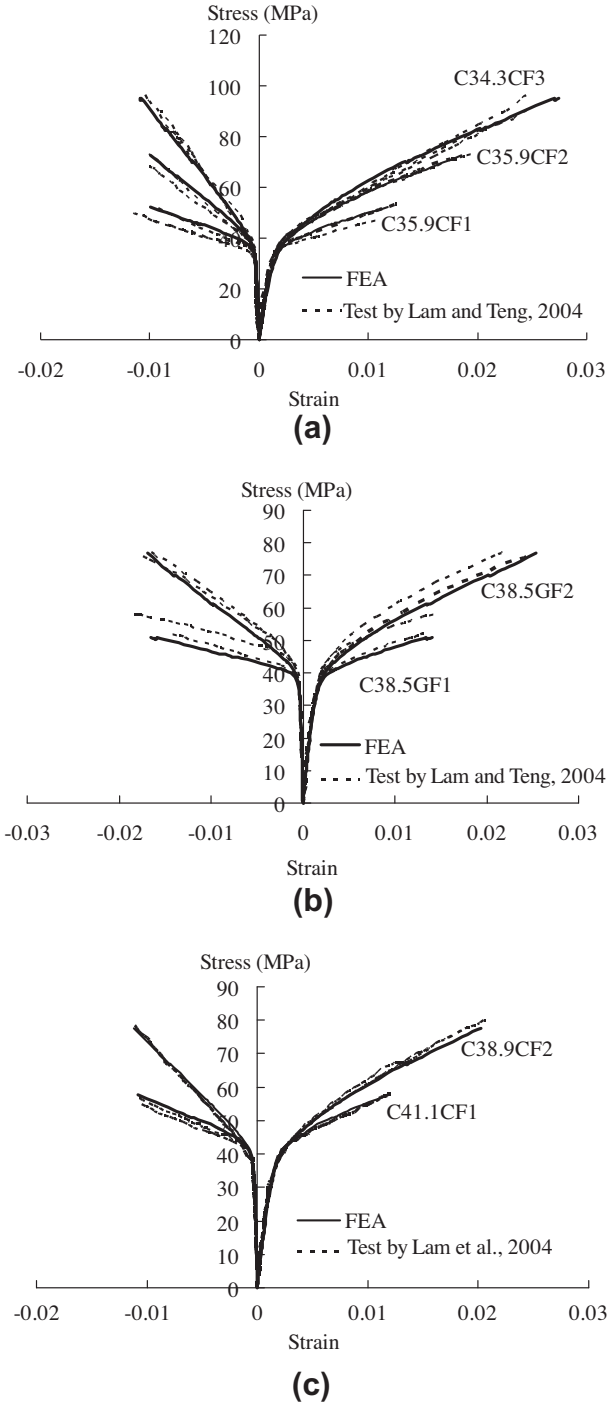

Fig. 18. Overall performance of the proposed models.

The friction model of Eq. (20) can also be validated from another perspective. The conventional strength model for confined concrete is given by Eq. (27) (Richart et al., 1928; Teng et al., 2007a; Wu and Wang, 2009; Wu and Zhou, 2010):

$$f_{cc}' = f_c' + k_e f_l, \tag{27}$$

where k_e is the confinement effectiveness coefficient, and f_{cc}' is the peak strength at lateral confinement f_l. Differentiating Eq. (1) with respect to p and considering Eq. (27) leads to

$$\tan\varphi = \frac{dt}{dp} = \frac{\delta(f'_{cc} - f_l)}{\delta\frac{(2f_l + f'_{cc})}{3}} = 3\frac{k_e - 1}{2 + k_e}. \quad (28)$$

where $\sigma_1 = f'_{cc}$ and $\sigma_2 = \sigma_3 = f_l$, and φ and k are considered as material constants in Eq. (1). The corresponding friction angle φ is calculated to be 53.7° from the model of Teng et al. (2007a), in which k_e is 3.5 for FRP confined concrete; it is 56.7° at $k = 4.1$ when the (Richart et al., 1928) model is adopted, which is suitable for actively confined concrete. In actively confined concrete, the initial confinement is much larger than in FRP confined columns for the same maximum confinement strength f_l. Therefore, the actively confined concrete experiences larger lateral restraint and hence smaller plastic dilation up to the onset of peak strength, leading to a smaller equivalent plastic strain than that for passively confined concrete. Based on Eq. (20), the friction angle for actively confined concrete is expected to be larger than that for FRP confined concrete, which well explains the difference between the two values calculated above.

5. Verification of the proposed model

5.1. Implementation in ABAQUS

For application, the proposed plastic dilation model (Eqs. (13)–(17)), friction angle model (Eq. (20)), and hardening/softening function (Eqs. (21)–(23)) are imported into ABAQUS through tabular data using SDFV option (ABAQUS, 2003). The concrete column is modeled as 1/8 of a cylinder with appropriate boundary conditions (Fig. 16), considering uniform deformation along the height and in circumferential direction. The FRP sheet is modeled as elastic laminar with orthotropic elasticity in plane stress without bending stiffness. Elastic modulus of FRP is only designated in the fiber direction and its corresponding Poisson's ratio is set as 0.3. There is no relative slip between the FRP and the concrete. The loading is under axial displacement control applied on the top of the column, without applying directly on the FRP. The concrete material is considered to be isotropic.

The model is verified by the database with 88 specimens in Table 3, including 29 specimens from Table 1 and additional 59 specimens tested by other researches. The overall range of unconfined concrete strength is from 31.4 MPa to 52.05 MPa. The ultimate strength and strain at FRP rupture are also calculated by the model, for all 88 specimens, and compared with test results in Table 3 and Fig. 17. The correlation coefficients are as high as 0.9832 and 0.9389 for the strength and the strain, respectively (Fig. 17). The average errors are 5.50% and 9.60% for the ultimate strength and the corresponding ultimate strain, respectively (Table 3). Considering the scattering of 5.9% in the strength and 16.6% in the strain of the test data, between different specimens in the same type of column, FEM results are considered well matched. Fig. 18 compares theoretical and experimental stress–strain response curves for the additional 19 specimens (7 types of column) tested by Lam and Teng (2004) and Lam et al. (2006) that were not used for deriving the model. Fig. 19 compares axial stress-axial strain curves (10 specimens) for the test results conducted by Karabinis and Rousakis (2002) and Eid et al. (2006). The good correlations demonstrate that the proposed model performs well for FRP confined circular concrete columns.

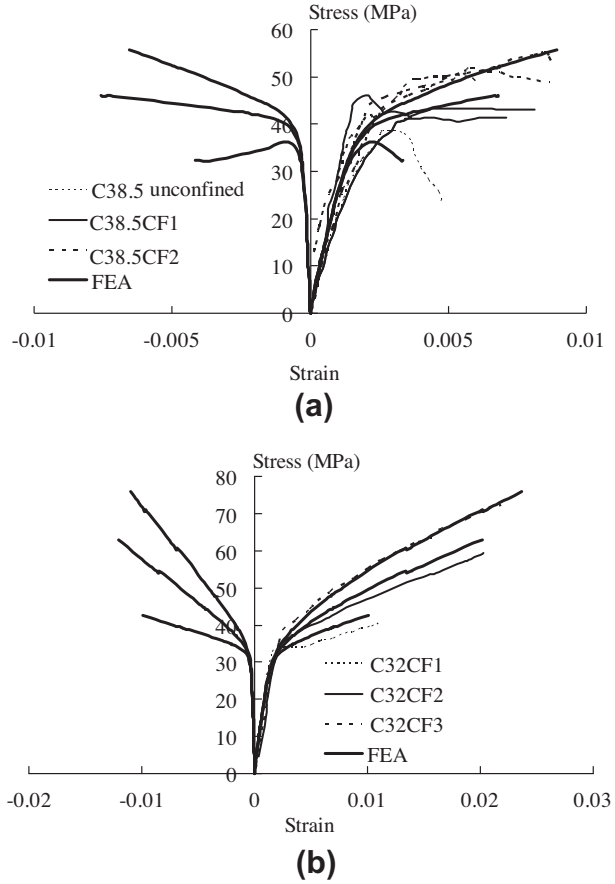

Fig. 19. Comparison of axial stress–strain curves: (a) specimens ($f'_c = 38.5$ MPa, $E_f = 240$ GPa, $t_f = 0.117$ mm, 0.234 mm) from Karabinis and Rousakis (2002), (b) specimens ($f'_c = 32$ MPa, $E_f = 78$ GPa, $t_f = 0.381$ mm, 0.762 mm, 1.143 mm) from Eid et al. (2006).

6. Conclusion

The friction angle, cohesion and plastic dilation are essential for the Drucker–Prager type material models. Through analytical studies of test results and FEM simulations using ABAQUS, explicit models for these properties were derived in this work. The model can be easily used for implementation in material models for numerical simulations of concrete materials and structures. The good agreement between test results and the model's prediction in stress–strain response curves demonstrates accuracy and effectiveness of the proposed model.

The database used to derive and verify the models includes 97 FRP confined column specimens, covering concrete grades from 31.4 MPa to 52.05 MPa and lateral stiffness ratios from 3.9 to 113.35. Strictly speaking the proposed model is only applicable within the above parameter ranges for normal-strength concrete in FRP confined circular columns under uniaxial loading. Care should be exercised in extending the model to cases outside the above parameter space, for example, to high strength concrete and columns with very high confinement levels.

Acknowledgments

The work described in this paper was fully supported by a grant from the Research Grants Council of the Hong Kong Special Administrative Region, China (Project No. CityU 123711). The authors would like to acknowledge the support from Professor JG Teng's group by way of providing the test data and in the use of ABAQUS.

References

ABAQUS, 2003. ABAQUS Analysis User's Manual, version 6.4.
Bullo, S. 2003. Experimental study of the effects of the ultimate strain of fiber reinforced plastic jackets on the behavior of confined concrete. In: Proceedings of the International Conference Composites in Construction, Cosenza, Italy, pp. 465–470.

Cui, C. 2009. Behaviour of normal and high strength concrete confined with fibre reinforced polymers (FRP), Ph.D thesis, Department of Civil Engineering, University of Toronto.

Dahl, K.K.B., 1992. A Failure criterion of for normal and high strength concrete. Department of Structural Engineering. Technical University of Demark.

Drucker, D.C., Prager, W., 1952. Soil mechanics and plastic analysis or limit design. Quart. Appl. Math. 10, 157–165.

Eid, R., Roy, N., Paultre, P. 2006. Behaviour of circular reinforced concrete columns confined with transverse steel reinforcement and fiber-reinforced composite sheets. In: Proceedings of 2nd fib Congress, Naples, Italy.

Grassl, P., Lundgren, K., Gylltoft, K., 2002. Concrete in compression: a plasticity theory with a novel hardening law. International Journal of Solids and Structures 39, 5205–5223.

Han, D.J., Chen, W.F., 1985. A nonuniform hardening plasticity model for concrete materials. Mechanics of Materials 4, 283–302.

Handin, J., 1969. On the Coulomb–Mohr failure criterion. Journal of Geophysical Research 74, 5343–5348.

Imran, I., Pantazopoulou, S.J., 2001. Plasticity model for concrete under triaxial compression. Journal of Engineering Mechanics-ASCE 127, 281–290.

Jiang, T., Teng, J.G., 2007. Analysis-oriented stress-strain models for FRP-confined concrete. Engineering Structures 29, 2968–2986.

Karabinis, A.I., Kiousis, P.D., 1996. Plasticity computations for the design of the ductility of circular concrete columns. Computers & Structures 60, 825–835.

Karabinis, A.I., Rousakis, T.C., 2002. Concrete confined by FRP material: a plasticity approach. Engineering Structures 24, 923–932.

Karabinis, A.I., Rousakis, T.C., Manolitsi, G.E., 2008. 3D finite-element analysis of substandard RC columns strengthened by fiber-reinforced polymer sheets. Journal of Composites for Construction 12, 531–540.

Lam, L., Teng, J.G., 2004. Ultimate condition of fiber reinforced polymer-confined concrete. Journal of Composites for Construction 8, 539–548.

Lam, L., Teng, J.G., Cheung, C.H., Xiao, Y., 2006. FRP–confined concrete under axial cyclic compression. Cement and Concrete Composites 28, 949–958.

Mahboubi, A., Ajorloo, A., 2005. Experimental study of the mechanical behavior of plastic concrete in triaxial compression. Cement and Concrete Research 35, 412–419.

Matthys, S., Taerwe, L., Audenaert., K. 1999. Tests on axially loaded concrete columns confined by fiber reinforced polymer sheet wrapping. In: Proceedings of the Fourth International Symposium on Fiber Reinforced Polymer Reinforcement for Reinforced Concrete Structures, ACI SP-188, Michigan, USA, pp. 217–219.

Mirmiran, A., Zagers, K., Yuan, W.Q., 2000. Nonlinear finite element modeling of concrete confined by fiber composites. Finite Elements in Analysis and Design 35, 79–96.

Oh, B. 2002. A plasticity for confined concrete under uniaxial loading, Ph.D thesis, Department of Civil Engineering, Lehigh University.

Papanikolaou, V.K., Kappos, A.J., 2007. Confinement-sensitive plasticity constitutive model for concrete in triaxial compression. International Journal of Solids and Structures 44, 7021–7048.

Pekau, O.A., Zhang, Z.X., Liu, G.T., 1992. Constitutive model for concrete in strain space. Journal of Engineering Mechanics 118, 1907–1927.

Popovics, S., 1973. A numerical approach to the complete stress-strain curve of concrete. Cement and Concrete Research 3, 583–599.

Richart, F.E., Brandtzaeg, A., Brown, R.L., 1928. A Study of the failure of concrete under combined compressive stresses. University of Illinois Bulletin, 26.

Ritchie, A.C.B., 1962. The triaxial testing of fresh concrete. Magazine of Concrete Research 14, 37–41.

Rousakis, T.C., Karabinis, A.I., Kiousis, P.D., Tepfers, R., 2008. Analytical modelling of plastic behaviour of uniformly FRP confined concrete members. Composites Part B-Engineering 39, 1104–1113.

Smith, S.S., William, K.J., Gerstle, K.H., Sture, S., 1989. Concrete over the top, or is there life after peak. ACI Materials Journal 86, 491–497.

Teng, J.G., Huang, Y.L., Lam, L., Ye, L.P., 2007a. Theoretical model for fiber-reinforced polymer-confined concrete. Journal of Composites for Construction 11, 201–210.

Teng, J.G., Yu, T., Wong, Y.L., Dong, S.L., 2007b. Hybrid FRP-concrete-steel tubular columns: concept and behavior. Construction and Building Materials 21, 846–854.

Vermeer, P.A., de Borst, R., 1984. Non-associated plasticity for soils, concrete and rock. Heron 29, 1–64.

Wang, L.M., Wu, Y.F., 2008. Effect of corner radius on the performance of CFRP-confined square concrete columns: test. Engineering Structures 30, 493–505.

Wu, Y.F., Wang, L.M., 2009. Unified strength model for square and circular concrete columns confined by external jacket. Journal of Structural Engineering (ASCE) 135, 253–261.

Wu, Y.F., Zhou, Y.W., 2010. A unified strength model based on Hoek–Brown failure criterion for circular and square concrete columns confined by FRP. Journal of Composites for Construction (ASCE) 14, 175–184.

Yu, T., Teng, J.G., Wong, Y.L., Dong, S.L., 2010. Finite element modeling of confined concrete-I: Drucker–Prager type plasticity model. Engineering Structures 32, 665–679.